Celastrol-Induced Weight Loss Is Driven by Hypophagia and Independent From UCP1

Katrin Pfuhlmann,[1,2,3,4] Sonja C. Schriever,[1,2,4] Peter Baumann,[1,2,3,4] Dhiraj G. Kabra,[4,5] Luke Harrison,[1,2,3,4] Sithandiwe E. Mazibuko-Mbeje,[2,4,6] Raian E. Contreras,[1,2,3,4] Eleni Kyriakou,[7,8] Stephanie E. Simonds,[9] Tony Tiganis,[9] Michael A. Cowley,[10] Stephen C. Woods,[11] Martin Jastroch,[2,4] Christoffer Clemmensen,[2,4] Meri De Angelis,[12] Karl-Werner Schramm,[12] Michael Sattler,[7,8] Ana C. Messias,[7,8] Matthias H. Tschöp,[2,3,4] and Paul T. Pfluger[1,2,4]

Diabetes 2018;67:2456–2465 | https://doi.org/10.2337/db18-0146

PHARMACOLOGY AND THERAPEUTICS

Celastrol, a plant-derived constituent of traditional Chinese medicine, has been proposed to offer significant potential as an antiobesity drug. However, the molecular mechanism for this activity is unknown. We show that the weight-lowering effects of celastrol are driven by decreased food consumption. Although young Lep^{ob} mice respond with a decrease in food intake and body weight, adult Lep^{db} and Lep^{ob} mice are unresponsive to celastrol, suggesting that functional leptin signaling in adult mice is required to elicit celastrol's catabolic actions. Protein tyrosine phosphatase 1 (PTP1B), a leptin negative-feedback regulator, has been previously reported to be one of celastrol's targets. However, we found that global PTP1B knockout (KO) and wild-type (WT) mice have comparable weight loss and hypophagia when treated with celastrol. Increased levels of uncoupling protein 1 (UCP1) in subcutaneous white and brown adipose tissue suggest celastrol-induced thermogenesis as a further mechanism. However, diet-induced obese UCP1 WT and KO mice have comparable weight loss upon celastrol treatment, and celastrol treatment has no effect on energy expenditure under ambient housing or thermoneutral conditions. Overall, our results suggest that celastrol-induced weight loss is hypophagia driven and age-dependently mediated by functional leptin signaling. Our data encourage reconsideration of therapeutic antiobesity strategies built on leptin sensitization.

Extracts of celastrol, a pentacyclic triterpenoid naturally occurring in the Chinese Thunder God vine *Tripterygium wilfordii*, are used in traditional Chinese medicine to treat fever, chills, joint pain, and edema. Recent evidence suggests that celastrol may be a novel antiobesity drug that mediates weight loss by acting as a leptin sensitizer (1).

Beneficial actions of chronic celastrol treatment against obesity and diabetes were first described by Kim et al. (2) and corroborated by Weisberg et al. (3), who observed lower body weight (BW) and blood glucose levels in leptin receptor–deficient Lep^{db} mice after treatment with 1 or 3 mg/kg BW celastrol, respectively. Because a single acute administration of intraperitoneal (i.p.) celastrol (3 mg/kg

[1]Research Unit Neurobiology of Diabetes, Helmholtz Zentrum München, Neuherberg, Germany
[2]Institute for Diabetes and Obesity, Helmholtz Zentrum München, Neuherberg, Germany
[3]Division of Metabolic Diseases, Technische Universität München, Munich, Germany
[4]German Center for Diabetes Research (DZD), Neuherberg, Germany
[5]Institute for Clinical Biochemistry and Pathobiochemistry, German Diabetes Center, Heinrich Heine University, Leibniz Center for Diabetes Research, Düsseldorf, Germany
[6]Biomedical Research and Innovation Platform, South African Medical Research Council, Tygerberg, South Africa
[7]Institute of Structural Biology, Helmholtz Zentrum München, Neuherberg, Germany
[8]Biomolecular Nuclear Magnetic Resonance and Center for Integrated Protein Science Munich at Department Chemie, Technische Universität München, Garching, Germany
[9]Department of Biochemistry and Molecular Biology, Monash University, Melbourne, Victoria, Australia
[10]Department of Physiology, Monash University, Melbourne, Victoria, Australia
[11]Psychiatry and Behavioral Neuroscience, Metabolic Diseases Institute, University of Cincinnati College of Medicine, Cincinnati, OH
[12]Molecular EXposomics, Helmholtz Zentrum München, Neuherberg, Germany
Corresponding author: Paul T. Pfluger, paul.pfluger@helmholtz-muenchen.de.

Received 31 January 2018 and accepted 3 August 2018.
This article contains Supplementary Data online at http://diabetes.diabetesjournals.org/lookup/suppl/doi:10.2337/db18-0146/-/DC1.

BW) improves glucose tolerance and insulin sensitivity in Lep^{db} mice compared with pair-fed Lep^{db} controls, the implication is that effects of celastrol on glucose homeostasis can be independent from the effects on BW and body composition (3).

Several mechanisms for celastrol's effects have been suggested. Using 10- to 30-fold lower doses, Liu et al. (1) reported celastrol to be a potent leptin sensitizer that inhibits food intake (FI), lowers BW, and improves glucose tolerance by reducing hypothalamic endoplasmic reticulum (ER) stress in diet-induced obese mice but not in lean mice or in leptin (receptor)-deficient Lep^{ob} or Lep^{db} mice. Celastrol administration decreased hepatic steatosis via increased Sirt1 expression in mice (4), and this led to impaired adipocyte differentiation but increased lipolysis in vitro in 3T3 adipocyte cells (5). Celastrol has also been suggested to decrease BW via the heat shock factor 1 (HSF1)–peroxisome proliferator–activated receptor γ coactivator 1-α (PGC-1α) axis and mitochondrial gene programs that lead to increased muscle and brown adipose tissue (BAT) thermogenesis and inguinal white adipose tissue (iWAT) browning (6).

Celastrol has several confirmed molecular targets. It inhibits IκB kinase (IKK)-α and IKK-β by binding to a cysteine (Cys) residue in the kinase activation loop (7). Celastrol further inhibits the interaction of Hsp90 with cochaperones such as cell division cycle 37 (Cdc37) by binding to Cys residues in Cdc37 (8,9) or to the dimer interface of Hsp90 (10), thereby destabilizing the Hsp90-Cdc37-IKK complex and inhibiting IKK signaling. In addition, celastrol directly inhibits proteasome activity (11), activates HSF1, and induces the heat shock response (12,13), but the molecular mechanisms are not known. Leptin-sensitizing properties of celastrol have been attributed to a decrease in ER stress, but direct molecular underpinnings remain elusive (1).

Our goal was to interrogate celastrol-induced weight loss by assessing celastrol's leptin-sensitizing molecular mechanism and its thermogenic potential. Special emphasis was given to the roles of protein tyrosine phosphatase (PTP) 1B (PTP1B) as a negative regulator of leptin action and to uncoupling protein 1 (UCP1) as a main driver for brown/beige fat thermogenesis. Our focus on PTP1B was driven by the following rationale: A recent experiment using triterpenoids reported inhibitory activity of celastrol toward several protein phosphatases, including PTP1B (14); and PTP1B is a known feedback regulator of insulin and leptin signaling via dephosphorylation of Janus kinase 2 (JAK2) (15), of the insulin receptor, and of insulin receptor substrate 1 (IRS1) (16). Our focus on UCP1 was driven by a recent report that attributed the weight-lowering effects of celastrol to the transcriptional activation of UCP1 with increased BAT activation, iWAT browning, and elevated energy expenditure (6).

RESEARCH DESIGN AND METHODS

Animals

C57BL/6J mice were obtained from Janvier Laboratories (Saint-Berthevin Cedex, France). UCP1 knockout (KO), Lep^{ob} and Lep^{db} mice on a C57BL/6J genetic background were originally provided from The Jackson Laboratory (Bar Harbor, ME) (strain names: B6.129-Ucp1tm1Kz/J; B6.Cg-Lepob/J/+; BKS.Cg-Dock7m $^{+/+}$ Leprdb/J). Global PTP1B KO mice (B6.129S4-Ptpn1^{tm1Bbk}/Mmjax) were a gift of Prof. Melanie Brinckmann (Helmholtz-Zentrum für Infektionsforschung GmbH, Braunschweig, Germany). All studies were performed in male mice, which were maintained on a 12-h dark-light cycle and had free access to diet and water. Mice were fed normal rodent chow (#1314; Altromin) or a 58% high-fat diet (HFD) (D12331; Research Diets). Celastrol (#34157-83-0; BOC Science, Shirley, NY) was dissolved in pure DMSO and diluted with PBS to a final concentration of 0.02 mg/mL in 1% DMSO for injections. Celastrol (100 μg/kg BW) or PBS with 1% DMSO as the vehicle was injected in a similar volume. HFD-fed diet-induced obesity (DIO) mice and chow-fed mice were injected i.p. UCP1 WT and KO mice, Lep^{ob} WT and KO mice, Lep^{db} WT and KO mice, and PTP1B WT and KO mice were injected subcutaneously (s.c.). Celastrol injections took place 1–2 h before dark onset. For post-portem analyses, mice were injected with 100 μg/kg BW celastrol or vehicle 1–2 h before sacrifice.

Mice were distributed into treatment groups based on their starting BW to ensure an equal distribution of starting BWs, allowing for better dissection of the effects of longitudinal treatments on BW. In vivo experiments were performed without blinding of the investigators. All studies were based on power analyses to assure adequate sample sizes and approved by the State of Bavaria, Germany.

Body Composition and Indirect Calorimetry

Fat and lean masses were assessed using nuclear magnetic resonance (NMR) technology (EchoMRI, Houston, TX). Energy expenditure, locomotor activity, and exact FI measurements were analyzed by a combined indirect calorimetry system (TSE System, Bad Homburg, Germany). Mice were acclimatized to the calorimetry system for at least 24 h before data collection for 3 days and 21 h at 23°C. To assess the effect of celastrol on basal metabolic rates and maximum respiration, housing temperatures were changed to 30°C for 17 h. Mice were subsequently injected with 0.5 μg/g BW norepinephrine (Sigma-Aldrich, St. Louis, MO) in 0.9% NaCl 2.5 h after light onset and assessed for the maximum increase in energy expenditure observed within 1 h. We determined the basal metabolic rates of vehicle and celastrol-treated mice housed at 30°C by averaging energy expenditure values from 4.5 to 6.5 h after light onset, a period when mice displayed the lowest daily physical activity. For the measurement of maximum respiration, one mouse was excluded due to a missed norepinephrine injection, and one mouse was excluded from FI analyses due to spillage.

Glucose Tolerance Tests

Mice were treated for 6 d with celastrol (100 μg/kg BW) or vehicle and then underwent a glucose tolerance test on day

7. After a 6 h fast, glucose (1.5 g/kg BW) was injected i.p., and tail blood glucose was measured using a handheld glucometer (FreeStyle Freedom Lite; Abbott Diabetes Care, Alameda, CA) before (0 min) and 15, 30, 60 and 120 min after the glucose injection.

RNA Isolation and Quantitative PCR Analysis

RNA was isolated from tissue using a commercially available kit (Macherey-Nagel, Düren, Germany). Equal amounts of RNA were transcribed to cDNA using the QuantiTect Reverse Transcription kit (Qiagen, Hilden, Germany). Gene expression was analyzed using custom-made primers (Sigma-Aldrich), TaqMan probes (Thermo Fischer Scientific, Rockford, IL), and SYBR Green or TaqMan Master Mix (Applied Biosystems, Carlsbad, CA). Gene expression was evaluated using the ΔΔCt method, and *Hprt* was used as the housekeeping gene. Primer pairs and TaqMan probes used are listed in the Supplementary Tables. Ct values for hypothalamic inflammatory markers were between 32 and 36.

Western Blotting and Densitometric Analyses

Radioimmunoprecipitation assay buffer containing protease and phosphatase inhibitor cocktail (Thermo Fisher Scientific) and 1 mmol/L phenylmethane sulfonyl fluoride (PMSF) were used for protein extraction. A Trans Blot Turbo transfer apparatus (Bio-Rad, Hercules, CA) transferred proteins from precast polyacrylamide gels (Bio-Rad) to nitrocellulose membranes. Membranes were incubated with anti-phosphorylated signal transducer and activator of transcription 3 ($pSTAT3^{T705}$) (rabbit polyclonal, 1:2,500; Cat #9145), anti-STAT3 (mouse monoclonal, 1:2,500; Cat #9139), anti-STAT5 (rabbit polyclonal, 1:1,000; Cat #9363), anti-UCP1 (rabbit monoclonal, 1:1,000; Cat #14670), and anti–β-actin (rabbit polyclonal, 1:20,000; Cat #4970). All antibodies were purchased from Cell Signaling Technology (Danvers, MA). Membranes were detected on an Odyssey Infrared Imaging System (LI-COR, Lincoln, NE) using enhanced chemiluminescence (Bio-Rad), and densitometric quantifications were performed using internal LI-COR Odyssey software.

Immunohistochemistry

Mice were perfused with PBS and a chilled 4% solution of paraformaldehyde in 0.1 mol/L PBS, and brains were extracted and incubated in fixative overnight on a shaker at 4°C. After incubation for 24–48 h with 30% sucrose in 0.1 mol/L Tris-buffered saline (TBS) at 4°C, brains were frozen at −20°C, coronally cut in a cryostat into 30-μm sections, and stored in a cryoprotectant solution containing glycerol, ethylene glycol, and sucrose dissolved in TBS. Staining was performed with free-floating slices and started by applying 2-h blocking in a buffer containing 0.25% gelatin and 0.5% Triton ×100 in 1× TBS. Primary anti-pSTAT3 goat (1:200, #sc7993; Santa Cruz Biotechnology) and anti-proopiomelanocortin (POMC; 1:500, H-029-30; Phoenix Pharmaceuticals) antibodies were diluted in blocking buffer and incubated overnight at 4°C. After several washing steps, Biotin-SP–conjugated AffiniPure Fab Fragment goat anti-mouse IgG (H+L) (1:500, #115-069-033; Jackson ImmunoResearch) was added to the slices in TBS for 1 h. After washing, streptavidin–Alexa Fluor 555 conjugate (1:500, #115-067-033; Life Technologies) and Alexa Fluor 488 goat anti-rabbit IgG (H+L) antibody (1:500, #A11008; Life Technologies) were added in TBS for 1 h and washed afterward several times. Z-stack images were captured by a Leica TCS SP8 microscope. Stack and overlay pictures were created using ImageJ 1.47 software.

The arcuate nucleus (ARC) was defined in each slice by orienting on DAPI and POMC staining as well as on the Allen Brain Atlas (http://mouse.brain-map.org/static/atlas). Green and red staining and green-red colocalizations in the ARC were counted, and pSTAT3 and POMC double-positive cells were normalized to the total number of POMC-positive cells in the ARC. Total numbers of pSTAT3- and POMC-positive cells were normalized to ARC area.

Liquid Chromatography Quantitative Time-of-Flight Mass Spectrometry

Celastrol was dissolved to a concentration of 0.08 mg/mL in the following solutions: *1*) pure DMSO, *2*) 50% DMSO in PBS, *3*) 10% DMSO in PBS, *4*) 5% DMSO in PBS, *5*) 45% 2-hydroxypropyl-β-cyclodextrin (cyclodextrin) containing DMSO (0.8 μL/mL) in PBS, or *6*) 45% cyclodextrin in PBS. The celastrol solutions were further diluted 1:400 and 1:800 with a mixture of H_2O:CH_3CN (1:1). Glycyrrhetinic acid was used as internal standard and dissolved in methanol to reach a concentration of 100 ng/μL. To each diluted solution, glycyrrhetinic acid was added to reach a final concentration of 2 ng/μL (dilution 1:400) or 1 ng/μL (dilution 1:800). All solutions containing the internal standard were analyzed with a nanoAcquity UPLC system (Waters, Milford, MA) that was connected to a quadrupole time-of-flight (Q-TOF 2) mass spectrometer (Waters Micromass, Manchester, U.K.). Compound separation was performed on a BEH C18 microscale column (300 μm internal diameter × 150 mm length, 1.7 μm particle size; Waters). The gradient high-performance liquid chromatography method used water (A) and acetonitrile (B) each containing 0.1% formic acid (vol/vol) as mobile phases. The gradient was as follows: 60% B held for 2 min, then increasing to 70% B in 1 min, and kept at 70% B for 7 min. The gradient then returned to the initial condition of 60% B over 1 min, which was held for 4 min to allow for equilibration before the next injection. Additional parameters were as follows: column temperature, 40°C; flow rate, 5 μL/min; injection volume, 5 μL. The Q-TOF was operated in electrospray negative ionization mode. The microchannel plate detector potential was 2,100 V, the capillary extraction voltage was 2.5 kV, and cone voltage was 70 V. High-purity nitrogen was used as the desolvation gas and auxiliary gas, and argon was used as the collision gas. The desolvation gas temperature was 120°C, and flow rate was 200 L/h. The cone gas flow rate was 50 L/h. The source temperature was 100°C. The collision energy was 25 eV. The instrumentation ran in full-scan mode with the Q-TOF

data collected over the range 100–1,000 m/z with a scan time of 2 s and interscan time of 0.1 s. Data acquisition and processing were performed on the QuanLynx Application Manager software (Waters-Micromass). The stability of celastrol was calculated based on the ratio between peak area internal standard divided by peak area celastrol. Every experiment was repeated in duplicates.

^{1}H-NMR

A 10 mmol/L (4.5 g/mL) stock solution of celastrol in pure deuterated DMSO (DMSO-d6) was prepared. From this stock the following solutions were prepared: *1*) celastrol at a final concentration of 177.5 μmol/L (0.08 mg/mL) in DMSO-d6; *2*) celastrol in PBS with 50% DMSO-d6; *3*) celastrol in PBS with 10% DMSO-d6, and *4*) celastrol in PBS with 5% DMSO-d6. The sample of 177.5 μmol/L celastrol in DMSO-d6 was used as the reference where the solubility of celastrol is considered 100%. Aliquots of all samples were subsequently incubated at 37°C, and measured at day 0, 7, and 14. Samples were then subjected to one-dimensional (1D) ^{1}H-NMR at 37°C on a Bruker 600 MHz spectrometer equipped with a QCI CryoProbe (^{1}H, ^{31}P, ^{13}C, ^{15}N) equipped with Z-gradients. 1D ^{1}H experiments were performed using a WATERGATE pulse sequence with 19 k time domain and 128 scans using 177.5 μmol/L celastrol samples in 100% DMSO-d6 and in PBS buffer (pH 7.4) and 5%, 10%, and 50% DMSO-d6. The solubility of celastrol was calculated based on the ratio between peak intensity of the aromatic proton 6 of celastrol in pure DMSO-d6 at time 0 divided by peak intensity of the same celastrol proton in PBS solution.

Statistical Analyses

Statistical analyses were performed using GraphPad Prism (GraphPad Software, La Jolla, CA) or SPSS (IBM, Armonk, NY) software. Untailed Student *t* test or two-way ANOVA with Bonferroni post test were applied to compare differences between phenotypes. Combined indirect calorimetry measurements were assessed by ANCOVA, using lean and fat mass as covariates. *P* values of <0.05 were considered significant. All results are presented as means ± SEM.

RESULTS

Celastrol Has Compromised Stability in Aqueous Solutions

To evaluate celastrol as a weight-loss agent in DIO mice, we first aimed to determine a formulation suitable for chronic in vivo injection studies. NMR revealed the highest stability and solubility when celastrol was dissolved in pure DMSO-d6 (Supplementary Fig. 1*A* and Supplementary Table 1) but decreasing stability and solubility when celastrol was dissolved under aqueous buffer conditions (PBS) with decreasing amounts of 50%, 10%, or 5% DMSO-d6 (Supplementary Fig. 1*B–D* and Supplementary Table 1) at 37°C and over a period of 14 days. Notably, despite adequate solubility at day 0, there was a dramatic drop in peak intensity and the appearance of new resonances for celastrol dissolved in PBS with 50% DMSO-d6 after 7 and 14 days of incubation (Supplementary Fig. 1*E–G*). The emergence of new peaks that increase in intensity over time, including in the aromatic region, points to reactions of celastrol with other molecules in solution, most likely with molecules resulting from the reaction of DMSO in aqueous solution (17). When celastrol was further diluted in PBS to 10% or 5% DMSO-d6, the occurrence of these additional peaks diminished, but the reduction of the parent compound was confounded with poor solubility. Liquid chromatography–mass spectrometry analyses confirmed the reduction in solubility and the poor stability of celastrol in aqueous buffers (Supplementary Table 2). Notably, by adding the complexing agent β-cyclodextrin (45% in PBS), we could increase the stability of celastrol incubated for 7 or 14 days at 37°C. Overall, however, the best solvent for celastrol appears to be 100% DMSO, because all tested aqueous solutions showed decreased stability at days 7 and 14 and/or decreased solubility at day 0. Pure DMSO is nevertheless toxic to mice, especially when given chronically. Accordingly, to minimize toxic side effects, we daily prepared fresh celastrol dissolved in 1% DMSO for all injection studies.

Celastrol Induces Hypophagia and Weight Loss

To identify the mechanism(s) by which celastrol achieves weight loss, we administered celastrol (100 μg/kg, i.p.) once daily for 6 days and observed significantly reduced BW, fat mass, and lean mass in HFD-fed DIO mice (Fig. 1*A* and *B* and Supplementary Fig. 2*A*) (age 36 ± 1 weeks; 32 weeks of HFD feeding) and chow-fed mice (Fig. 1*C* and *D* and Supplementary Fig. 2*B*) (age 36 ± 1 weeks). Celastrol treatment reduced FI in DIO mice (Fig. 1*E*), and there was a trend in the same direction in chow-fed mice (Fig. 1*F*). The decrease in FI in DIO mice was delayed, with maximum efficacy occurring 9–12 h after celastrol administration (Supplementary Fig. 2*C–E*), suggesting a celastrol-dependent alteration of gene expression. Decreased respiratory exchange ratios and locomotory patterns were temporally correlated with reduced FI (Supplementary Fig. 2*F–H*). Overall, we observed proportionally greater weight loss in direct linear correlation to BW in all mice tested, regardless of chow or HFD feeding (Fig. 1*G*) (i.e., heavier mice lost the most weight, and lean mice lost little to no weight).

Celastrol-Induced Weight Loss Requires Functional Leptin Signaling in Adult Mice

Contrary to reports using 10- to 30-fold higher doses (2,3), but consistent with the findings of Liu et al. (1), celastrol (100 μg/kg) did not decrease BW, fat, or lean mass in 8-week-old chow-fed leptin receptor-deficient Lep^{db} mice (Fig. 2*A–C* and Supplementary Fig. 3*A*). Functionality of celastrol was confirmed by a reduction of BW (Fig. 2*A*) and fat and lean mass (Fig. 2*C*) in age-matched chow-fed lean C57Bl/6J (WT) controls with a mean BW of 23.5 g (Supplementary Fig. 3*A*). Similarly, celastrol had no weight loss efficacy in 14-week-old chow-fed leptin-deficient Lep^{ob}

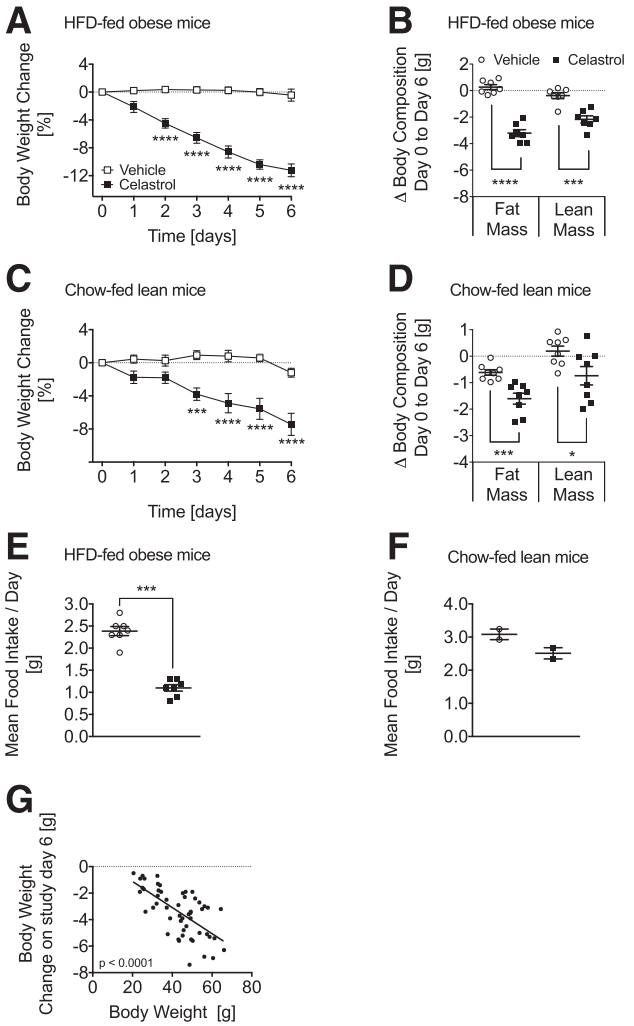

Figure 1—Celastrol decreases BW in chow- and HFD-fed mice. DIO mice (age 36 ± 1 weeks, fed the HFD for 32 weeks) treated daily with celastrol (100 μg/kg BW; i.p.; n = 7) or vehicle (n = 7) for 6 days displayed BW loss (*A*) and fat and lean mass loss (*B*). *C* and *D*: Chow-fed C57BL/6J mice (age 36 ± 1 weeks) were treated daily with 100 μg celastrol/kg BW or vehicle (i.p.) for 6 days. BW changes (*C*) and changes in body composition (*D*) in chow-fed mice (n = 8). Mean daily FI was assessed over a period of 6 days in DIO mice (seven cages) (*E*) and chow-fed C57BL/6J mice (two cages) (*F*) treated daily with celastrol (100 μg/kg BW) or vehicle (i.p.). *G*: Correlation of BW changes on study day 6 and the initial BW at day 0 in mice injected with celastrol (100 μg/kg, BW; n = 53). Two-way ANOVA with Bonferroni post hoc tests were applied for *A* and *C*. Unpaired Student t tests were used for statistical analyses of data in *B*, *D*, and *E*. Linear regression was applied for *G*. Means ± SEM; $^*P < 0.05$; $^{***}P < 0.001$; $^{****}P < 0.0001$.

mice, but decreased BW, fat, and lean mass in age-matched chow-fed WT controls (Fig. 2*D*–*F*) with a BW of 30.6 g (Supplementary Fig. 3*B*). Celastrol treatment for 6 days further improved glucose tolerance in chow-fed WT mice but not in celastrol-injected Lep^{ob} mice (Fig. 2*G* and *H*).

To assess whether effects of 100 μg/kg celastrol on BW, FI, and body composition are indeed strictly leptin-dependent, we administered vehicle or leptin to a group of young (age 6 week) chow-fed Lep^{ob} mice (Supplementary Fig. 3*C*). In contrast to what occurred in aged mice, there was reduced weight gain in Lep^{ob} mice treated with celastrol compared with vehicle-treated Lep^{ob} mice, and this was reflected by significantly reduced fat and lean mass (Supplementary Fig. 3*D* and *E*). These celastrol-treated Lep^{ob} mice also had reduced FI compared with vehicle-treated controls (Supplementary Fig. 3*F*). Our data are thus consistent with an earlier report that shows temporary weight reduction in young Lep^{ob} mice (1), indicating that celastrol's leptin-sensitizing activity may be age dependent. Alternatively, because young Lep^{db} mice had no weight loss in response to celastrol treatment (Fig. 2*B* and Liu et al. [1]), it appears plausible that celastrol may temporarily increase the constitutive activity of the long isoform of leptin receptor (LepRb) or its affinity for alternative cytokines (1).

To identify celastrol's first-order targets, we next assessed key hypothalamic signaling networks that orchestrate glucose and energy homeostasis. Surprisingly, celastrol administration to DIO mice (age 36 ± 1 weeks, 32 weeks of the HFD) significantly increased Agouti-related protein (AgRP) mRNA expression but had no effect on mRNA expression of other neuropeptides and components of leptin and melanocortin signaling (Supplementary Fig. 4*A* and *B*). Moreover, celastrol had little effect on mRNA levels of genes involved in hypothalamic ER stress and hypothalamic inflammation (Supplementary Fig. 4*C*). The nearly identical and somewhat paradoxical increase in hypothalamic AgRP expression after celastrol treatment has already been reported by Liu et al. (1), which makes it unlikely to be a coincidence or artifact. Rather, it might be a counterregulatory response to the negative energy balance of celastrol-treated mice. Overall, however, the reason for the increase in AgRP mRNA levels remains elusive.

Celastrol administration did not lead to an additional activation of leptin-responsive neurons in the hypothalamus, as revealed by similar numbers of pSTAT3-positive POMC neurons (Fig. 3*A* and *B*). Nevertheless and consistent with the data of Liu et al. (1), phosphorylation levels of the leptin target STAT3 (Fig. 3*C* and *D*), as well as basal STAT3 and STAT5 protein levels (Fig. 3*C* and *E*), were elevated in celastrol-injected mice. These data imply that celastrol may drive the further activation of leptin-responsive POMC neurons or induce the recruitment and activation of additional LepRb-expressing neuronal subpopulations in the hypothalamus. The exacerbation of leptin signaling in leptin-responsive neurons could be facilitated by a direct celastrol-driven disruption of JAK-STAT feedback inhibition.

Celastrol-Induced Weight Loss Is Unperturbed by Global PTP1B Deletion

JAK-STAT feedback inhibition is mediated by PTPs, which are long-recognized antiobesity drug targets (18). PTP1B was the first PTP linked to leptin signaling (19), and the PTP1B inhibitor and leptin sensitizer trodusquemine shares structural similarities with celastrol (20). We thus assessed whether celastrol mediates leptin resensitization

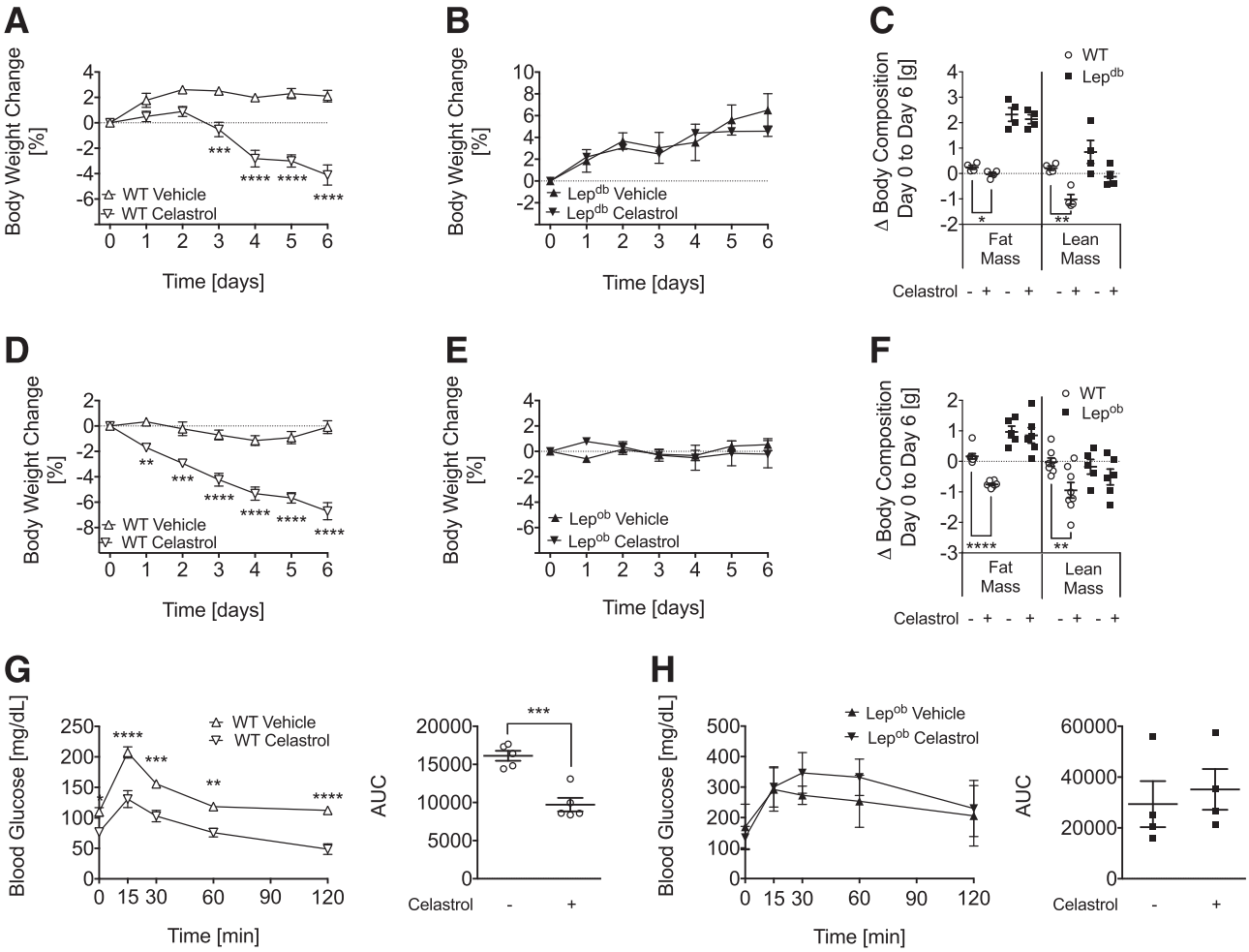

Figure 2— Celastrol-induced weight loss is leptin dependent. BW changes in chow-fed and age-matched lean C57Bl/6J (WT; age 8 weeks) (*A*) and leptin receptor–deficient obese Lep^{db} mice (*B*) treated with celastrol (100 μg/kg BW/day, s.c.; WT: $n = 4$, Lep^{db}: $n = 4$) or vehicle (WT: $n = 4$, Lep^{db}: $n = 4$) for 6 days, and changes in body composition (*C*). Changes in BW (*D* and *E*), body composition (*F*), and glucose tolerance (*G* and *H*) in chow-fed and age-matched C57Bl/6J (WT; age 14 ± 2 week) and leptin-deficient obese Lep^{ob} mice fed the chow diet and treated with celastrol (100 μg/kg BW/day, s.c.; WT: $n = 8$, Lep^{ob}: $n = 6$) or vehicle (WT: $n = 8$, Lep^{ob}: $n = 5$–6) for 6 days. Mice in *G* and *H* received an intraperitoneal bolus of 2 g/kg BW glucose (WT: $n = 5$, Lep^{ob}: $n = 4$). AUC, area under the curve. Two-way ANOVA with Bonferroni post hoc tests were applied to *A*, *B*, *D*, *E*, *G* (left panel), and *H* (left panel). Unpaired Student *t* tests were used for *C*, *F*, *G* (right panel), and *H* (right panel). Means ± SEM. $^*P < 0.05$; $^{**}P < 0.01$; $^{***}P < 0.001$; $^{****}P < 0.0001$.

via inhibition of PTP1B. We first assessed celastrol-induced weight loss in PTP1B WT and KO littermates with similar initial BWs (Supplementary Fig. 4*D*) that were fed the chow diet (age 22 ± 7 weeks). Chow-fed PTP1B KO mice had more weight loss with celastrol treatment than WT littermates (Fig. 3*F*), and this was accompanied by nonsignificant decreases in fat and lean mass in PTP1B KO mice and a significant loss of lean mass in WT mice (Fig. 3*G*). Similarly, when the same cohort of mice was subsequently fed the HFD for 10 weeks, celastrol induced weight loss in both PTP1B WT and KO mice (Fig. 3*H*), and this was largely explained by concomitant decreases in fat and lean mass (Fig. 3*I*). Notably, in contrast to earlier studies (21,22) reporting protection from DIO in PTP1B-deficient mice, we observed similar BWs; that is, there was a similar propensity for DIO in WT and PTP1B littermates fed the HFD for 10 weeks (Supplementary Fig. 4*E*).

Celastrol-Induced Weight Loss Is Independent From UCP1-Driven Thermogenesis

We next assessed whether celastrol can facilitate weight loss via UCP1-mediated mitochondrial uncoupling in adipose tissue. Consistent with a recent report (6), celastrol led to upregulated gene expression of medium-chain acyl-CoA dehydrogenase (*Mcad*) and *Ucp1* in BAT and of HSF1 (*Hsf1*) and UCP1 (*Ucp1*) in iWAT (Fig. 4*A*), as well as to higher UCP1 protein levels in BAT (Fig. 4*B*). However, transcription of *Pgc1-α* and key thermogenic genes was unaffected in iWAT and BAT (Supplementary Fig. 5*A* and *B*). Celastrol had also no cell-autonomous thermogenic effects on C2C12 muscle cells in vitro (Supplementary Fig. 5*C* and *D*) and did not induce mitochondrial genes or genes involved in nonshivering thermogenesis in skeletal muscle in vivo (Supplementary Fig. 5*E* and *F*).

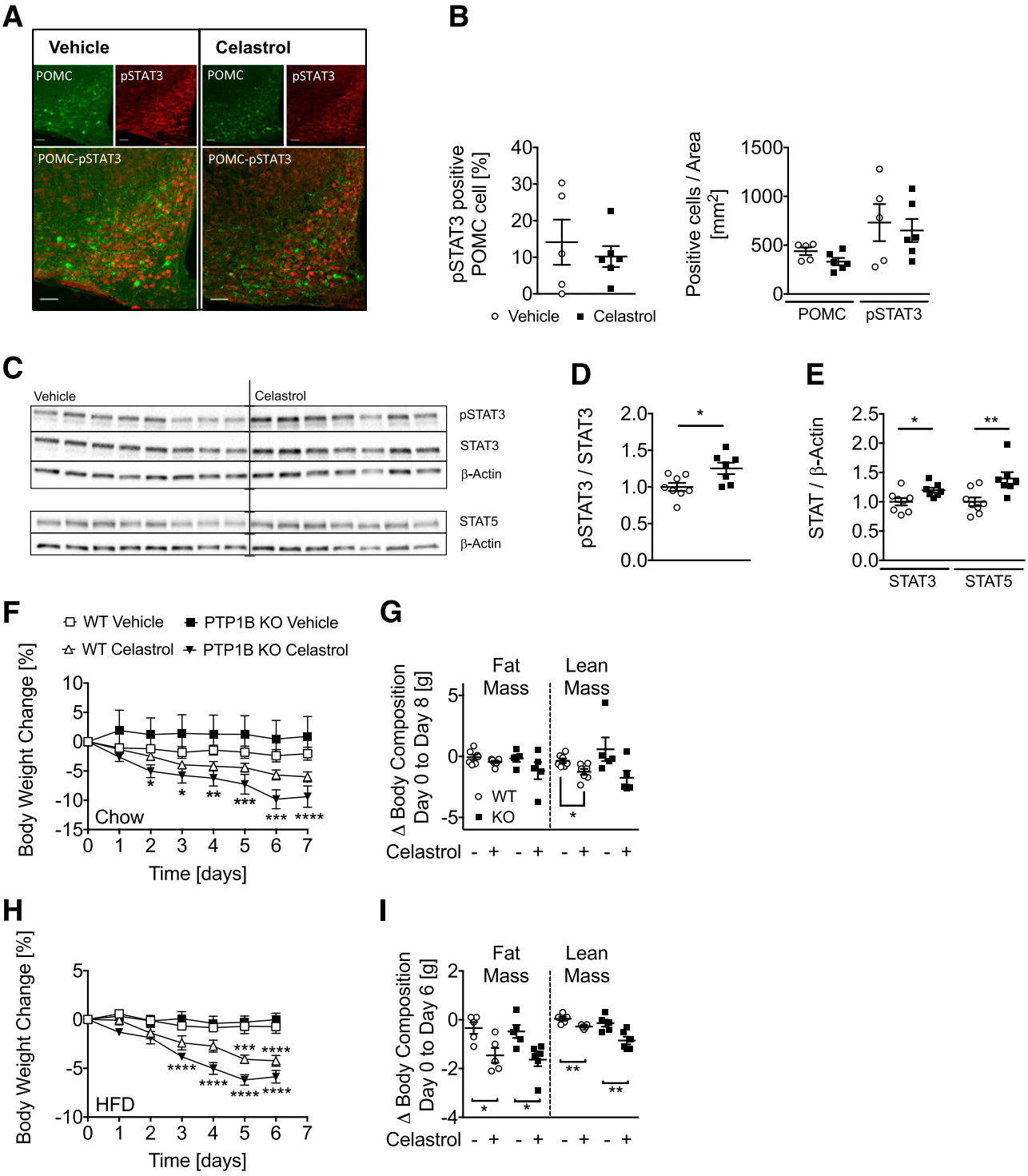

Figure 3—Celastrol increases hypothalamic pSTAT3 as well as basal STAT3 and STAT5 protein levels, but celastrol-induced weight loss is independent from PTP1B. Hypothalamic slices of HFD-fed C57BL/6J mice (age 36 ± 3 weeks) injected with celastrol (100 μg/kg BW/day) or vehicle for 6 days (i.p.) were immunostained with anti-POMC and anti-pSTAT3 antibody (scale bars, 50 μm) (*A*) and assessed for the percentage of pSTAT3-positive POMC cells (*B*, left panel) or the number of POMC or pSTAT3-positive cells per area (n = 5–6) (*B*, right panel). Western blot (*C*) and densitometric analyses of pSTAT3, normalized to total STAT3) (*D*) or basal STAT3 and STAT5 (normalized to β-actin) (*E*) protein levels in hypothalami of celastrol (100 μg/kg BW/day) or vehicle-treated mice (i.p.; n = 7–8). Changes in BW (*F*) and body composition (*G*) in chow-fed global PTP1B-KO mice and WT littermates (age 22 ± 7 weeks) treated with celastrol (100 μg/kg BW/day, i.p.; WT: n = 6, PTP1B KO: n = 5) or vehicle (WT: n = 7, PTP1B KO: n = 5; one vehicle-injected PTP1B-KO animal was identified as a significant outlier with a Grubbs test and was excluded) for 7 days. Celastrol-induced weight loss (*H*) and body composition changes (*I*) were further tested in global PTP1B-KO mice and WT littermates that were fed the HFD for 10 weeks and received 1 week of celastrol injections (100 μg/kg BW, i.p.; WT: n = 7, PTP1B KO: n = 5) or vehicle (WT: n = 7, PTP1B KO: n = 5). Unpaired Student t tests were used for *B*, *D*, *E*, *G*, and *I*. Two-way ANOVA with Bonferroni post hoc tests were applied to *F* and *H*. Means ± SEM. $^*P < 0.05$; $^{**}P < 0.01$; $^{***}P < 0.001$; $^{****}P < 0.0001$.

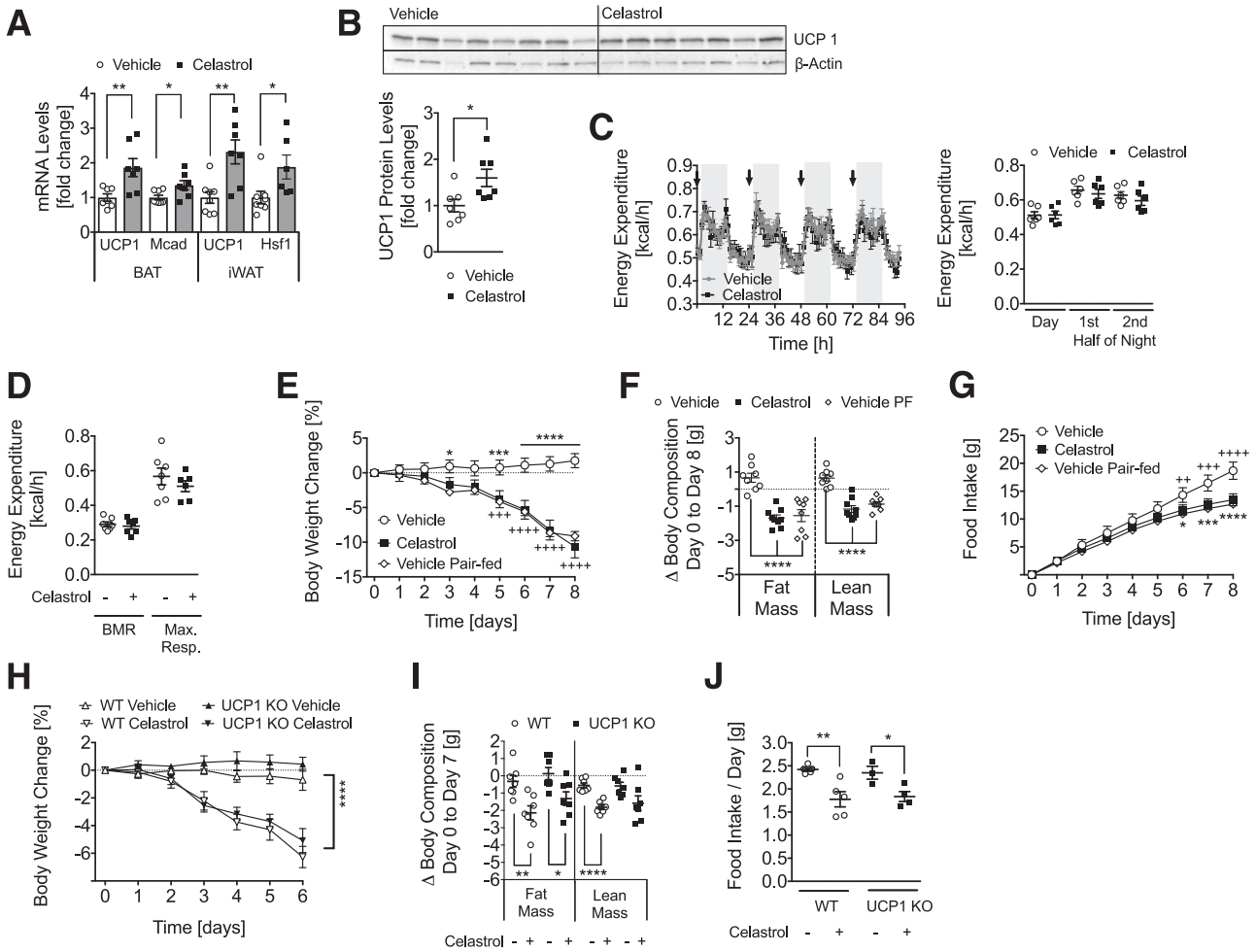

Figure 4— Celastrol decreases BW independent from UCP1 and has no effect on energy expenditure. *A*: mRNA levels of genes (*Ucp1*, *Mcad*, *Hsf1*) involved in browning, β-oxidation, and heat shock response in BAT and iWAT of celastrol vs. vehicle-treated DIO mice ($n = 7$, 6-day i.p. injection, 100 μg/kg). *B*: Protein levels of UCP1 in BAT of celastrol vs. vehicle-treated (i.p.) DIO mice, depicted by Western blot and densitometry analyses ($n = 7$–8, 6-day i.p. celastrol injection, 100 μg/kg BW). *C*: Unperturbed energy expenditure at ambient room temperature in HFD-fed DIO mice injected daily (indicated by arrows) with celastrol (100 μg/kg BW) or vehicle for 4 days ($n = 6$). *D*: Additional indirect calorimetry measurements of celastrol (100 μg/kg BW/day, i.p.) and vehicle-injected mice further revealed unchanged basal metabolic rates (BMR) and maximal respiratory capacities (Max. Resp.) after a single injection of norepinephrine (0.5 μg/g BW) under thermoneutral conditions ($n = 7$). Pair-feeding (PF) of HFD-fed and vehicle-treated DIO mice (age 16 weeks) to the amount of food consumed by celastrol-treated (100 μg/kg BW/day) DIO mice led to a similar reduction in BW (*E*) as well as fat and lean mass (*F*) compared with ad libitum fed and vehicle-treated DIO mice, indicating that the reduction of FI (*G*; three to five cages) is solely responsible for celastrol-induced weight loss. DIO-WT and UCP1-KO mice (age 44 ± 4 weeks) injected with celastrol (100 μg/kg BW/day s.c.; WT: $n = 7$, KO: $n = 7$) or vehicle (WT: $n = 7$, KO: $n = 7$) for 6 days displayed BW loss (*H*), fat and lean mass loss (*I*), and decreased daily FI (*J*) (three to seven cages). Unpaired Student *t* tests were used for *A*–*C* (right panel), *D*, *I*, and *J*. One-way ANOVA was applied for *F*. Two-way ANOVA with Bonferroni post hoc tests was applied for *E*, *G*, and *H*. ANCOVA was applied on *C* and *D*. Means ± SEM. $^{*}P < 0.05$, $^{**}P < 0.01$, $^{***}P < 0.001$, $^{****}P < 0.0001$ celastrol vs. vehicle (*A*, *B*, *E*, and *G*–*J*) or vehicle vs. vehicle pair-fed (*F*), $^{++}P < 0.01$, $^{+++}P < 0.001$, $^{++++}P < 0.0001$ vehicle vs. vehicle pair-fed (*E* and *G*).

Despite elevated UCP1 levels in iWAT and BAT, celastrol treatment had no effect in DIO mice on energy expenditure, basal metabolic rate, or maximal norepinephrine-induced respiration under ambient housing or thermoneutral conditions of 23°C and 30°C, respectively (Fig. 4*C* and *D*) (age 24 weeks, 20 weeks of the HFD). Similarly, pair-feeding vehicle-treated DIO mice to the average food consumption of celastrol-treated DIO mice resulted in the same decrease in BW (Fig. 4*E* and Supplementary Fig. 5*G*) and in fat and lean mass (Fig. 4*F*), compared with ad libitum fed vehicle-treated DIO mice (age 16 weeks, 12 weeks of the HFD). These data suggest that the reduction of FI (Fig. 4*G*) is likely the main driver for celastrol-induced loss of lean mass, thus arguing against putative toxic effects of celastrol on lean mass. Moreover, DIO UCP1-deficient mice and isogenic DIO WT mice had comparably decreased BW, fat mass, and FI in response to celastrol administration (Fig. 4*H*–*J* and Supplementary Fig. 5*H*) (age 44 ± 4 weeks, 34 weeks of the HFD). Collectively, these results strongly argue that celastrol-induced BW reduction is not mediated by UCP1-mediated mitochondrial uncoupling and thermogenesis.

DISCUSSION

Ideal treatment strategies against obesity will entail both a reduction in FI and the expenditure of excessive energy via thermogenesis. Although the former is a centrally mediated process, the latter results from increased heat production by peripheral thermogenic tissues such as white or brown adipose tissue and skeletal muscle. Celastrol has recently emerged as a promising antiobesity drug that can induce hypophagia due to unprecedented in vivo leptin resensitization properties (1) as well as to iWAT browning and BAT UCP1 levels (6). Our results are consistent with these reports, revealing a concomitant increase in UCP1 levels in iWAT and BAT of mice treated with celastrol and celastrol-induced weight loss that is due to a partially leptin-dependent decrease in food consumption. However, follow-up experiments revealed comparable BW loss and hypophagia in UCP1 KO and WT mice treated with celastrol, implying that UCP1-mediated thermogenesis is not a major driver for the BW-lowering effects of celastrol.

The lack of celastrol-induced weight loss in adult Lep^{ob} and Lep^{db} mice suggests that celastrol-induced reduction of FI is strictly leptin-dependent. Nevertheless, we found considerable celastrol-induced hypophagia and weight loss in 6-week-old leptin-deficient mice. This is consistent with a previous report of metabolic improvements of celastrol administered at a higher dose (1 mg/kg BW, i.p.) in 8-week-old leptin receptor-deficient Lep^{db} mice (2) or with a temporary weight loss in young Lep^{ob} mice, which nevertheless disappeared after prolonged low-dose celastrol treatment (1). These data highlight the plurality of celastrol's catabolic actions, which may include the sensitization of central nervous system (CNS) LepRb signaling as well as nonleptin-driven mechanisms. In this context, one should further note that our current definition of leptin resistance is largely based on the failure of exogenous leptin to reduce FI and BW. On a molecular level, however, the definition of leptin resistance largely remains an enigma, with one recent report even questioning the existence of resistance against endogenous leptin signaling (23).

A putative molecular player in the development of leptin resistance is leptin negative feedback regulator PTP1B. Celastrol was recently reported to have direct inhibitory activity against PTP1B in an in vitro phosphatase assay (14). However, we found celastrol-induced weight loss in both WT and global PTP1B-deficient mice, indicating that there are PTP1B-independent mechanisms of celastrol action. However, the high sequence homology between PTP1B and T-cell PTP (TCPTP) makes it plausible that TCPTP is also a target of celastrol. This also resonates with recent studies demonstrating that only a concomitant deletion of PTP1B and TCPTP signaling in POMC neurons blocks hypothalamic leptin actions on iWAT browning and BAT activation (24). Accordingly, our findings of iWAT browning and BAT UCP1 expression may point to a concomitant inhibition of both PTP1B and TCPTP by celastrol. Compensatory hypothalamic TCPTP signaling could explain the unperturbed weight loss efficacy of celastrol in global PTP1B KO mice. However, whether celastrol indeed inhibits TCPTP remains to be tested by in vitro binding assays or in vivo murine loss-of-function models.

Hypophagia as the main driver for celastrol-induced weight loss implicates the CNS as the primary celastrol target tissue. Specifically, CNS centers governing leptin-dependent ingestive behaviors appear to be the most promising sites of celastrol action. Future studies should delineate the relative contribution of these CNS areas for celastrol action. Celastrol's chemical instability in aqueous buffers, especially in the presence of DMSO to increase its solubility may, however, complicate chronic studies on the catabolic actions of celastrol in the CNS. Such studies on CNS celastrol actions may be directed toward leptin-melanocortin signaling in hypothalamic AgRP and/or POMC neurons, but neurocircuitry outside the hypothalamus could be of equal importance. Future studies will help distinguish celastrol's direct effects on the CNS from indirect effects caused by celastrol-induced weight loss or from potentially direct effects against peripheral targets such as pancreatic β-cells (3).

In summary, our results in UCP1 loss-of-function models argue against celastrol-induced iWAT or BAT browning and UCP1-dependent or -independent thermogenesis (25–28) as being the primary cause of the observed weight loss due to celastrol. Rather, the major effect of celastrol on weight loss appears to be driven via the CNS control of FI. Age or a putative sensitization of LepRb signaling appear to be key factors for the lack of catabolic actions of celastrol in adult mice but for normal weight loss in young Lep^{ob} mice. However, the mode of action and exact role of leptin signaling remain elusive. Overall, we corroborate the considerable potential of celastrol as an antiobesity drug. A pair-feeding study revealed that the loss of body adiposity and minor loss of lean mass after celastrol treatment was solely driven by a reduction in FI. Accordingly, celastrol appears safe and efficacious in preclinical models of obesity and in lean mice. These discoveries encourage reconsideration of leptin sensitizers as drugs against metabolic dysfunction. Moreover, by delineating the molecular action of celastrol, we may be able to shed new light on the enigma that is leptin resistance.

Acknowledgments. The authors thank Emily Baumgart, Heidi Hofmann, Laura Sehrer, and Luisa Müller (Helmholtz Zentrum München, Munich, Germany) for their skillful technical assistance.

Funding. This work was partly supported by the Helmholtz Alliance ICEMED-Imaging and Curing Environmental Metabolic Diseases (S.C.S. and M.H.T.), the Marie Skłodowska Curie training network "ChroMe" (grant H2020-MSCA-ITN-2015-675610, R.E.C., M.H.T., and P.T.P.), the Alexander von Humboldt Foundation (M.H.T.), the National Heart Foundation of Australia (S.E.S.) and National Health and Medical Research Council Australia (grant 1107336 to S.E.S. and grant 1079422 to M.A.C.), an intramural Diabetes Portfolio Grant (M.S. and A.C.M.), the Helmholtz Portfolio Program "Metabolic Dysfunction" (M.S. and M.H.T.), the Helmholtz Initiative for Personalized Medicine (iMed, M.H.T.), the Helmholtz-Israel-Cooperation in Personalized Medicine (P.T.P.), and through the Initiative and Networking Fund of the Helmholtz Association.

Duality of Interest. M.H.T. is a scientific advisor to Novo Nordisk and ERX. No other potential conflicts of interest relevant to this article were reported.

Author Contributions. K.P. performed quantitative PCR and Western blot analyses. K.P., S.C.S., P.B., D.G.K., L.H., R.E.C., C.C., and P.T.P. performed in vivo experiments in mice. K.P., S.C.S., D.G.K., E.K., S.E.S., T.T., M.A.C., S.C.W., C.C., M.D.A., K.-W.S., M.H.T., and P.T.P. designed experiments and analyzed and interpreted the results. K.P. and P.B. conducted immunohistochemical staining. K.P., E.K., T.T., M.A.C., S.C.W., A.C.M., M.H.T., and P.T.P. prepared the manuscript. S.C.S., A.C.M., M.H.T., and P.T.P. developed the conceptual framework of this study. S.E.M.-M. and M.J. performed in vitro experiments in C2C12 cells. E.K., M.S., and A.C.M. performed 1D ^{1}H-NMR experiments. M.D.A. and K.-W.S. conducted liquid chromatography quantitative time-of-flight mass spectrometry measurements. P.T.P. is the guarantor of the study and, as such, had full access to all the data and takes responsibility for the integrity of the data and the accuracy of the data analysis.

References

1. Liu J, Lee J, Salazar Hernandez MA, Mazitschek R, Ozcan U. Treatment of obesity with celastrol. Cell 2015;161:999–1011
2. Kim JE, Lee MH, Nam DH, et al. Celastrol, an NF-κB inhibitor, improves insulin resistance and attenuates renal injury in db/db mice. PLoS One 2013;8:e62068
3. Weisberg S, Leibel R, Tortoriello DV. Proteasome inhibitors, including curcumin, improve pancreatic β-cell function and insulin sensitivity in diabetic mice. Nutr Diabetes 2016;6:e205
4. Zhang Y, Geng C, Liu X, et al. Celastrol ameliorates liver metabolic damage caused by a high-fat diet through Sirt1. Mol Metab 2016;6:138–147
5. Choi SK, Park S, Jang S, et al. Cascade regulation of PPARγ(2) and C/EBPα signaling pathways by celastrol impairs adipocyte differentiation and stimulates lipolysis in 3T3-L1 adipocytes. Metabolism 2016;65:646–654
6. Ma X, Xu L, Alberobello AT, et al. Celastrol protects against obesity and metabolic dysfunction through activation of a HSF1-PGC1α transcriptional axis. Cell Metab 2015;22:695–708
7. Lee JH, Koo TH, Yoon H, et al. Inhibition of NF-kappa B activation through targeting I kappa B kinase by celastrol, a quinone methide triterpenoid. Biochem Pharmacol 2006;72:1311–1321
8. Sreeramulu S, Gande SL, Göbel M, Schwalbe H. Molecular mechanism of inhibition of the human protein complex Hsp90-Cdc37, a kinome chaperone-cochaperone, by triterpene celastrol. Angew Chem Int Ed Engl 2009;48:5853–5855
9. Jiang F, Wang HJ, Bao QC, et al. Optimization and biological evaluation of celastrol derivatives as Hsp90-Cdc37 interaction disruptors with improved druglike properties. Bioorg Med Chem 2016;24:5431–5439
10. Peng B, Gu YJ, Wang Y, et al. Mutations Y493G and K546D in human HSP90 disrupt binding of celastrol and reduce interaction with Cdc37. FEBS Open Bio 2016;6:729–734
11. Yang H, Landis-Piwowar KR, Chen D, Milacic V, Dou QP. Natural compounds with proteasome inhibitory activity for cancer prevention and treatment. Curr Protein Pept Sci 2008;9:227–239
12. Westerheide SD, Bosman JD, Mbadugha BNA, et al. Celastrols as inducers of the heat shock response and cytoprotection. J Biol Chem 2004;279:56053–56060
13. Trott A, West JD, Klaić L, et al. Activation of heat shock and antioxidant responses by the natural product celastrol: transcriptional signatures of a thiol-targeted molecule. Mol Biol Cell 2008;19:1104–1112
14. Scott LM, Chen L, Daniel KG, et al. Shp2 protein tyrosine phosphatase inhibitor activity of estramustine phosphate and its triterpenoid analogs. Bioorg Med Chem Lett 2011;21:730–733
15. Myers MP, Andersen JN, Cheng A, et al. TYK2 and JAK2 are substrates of protein-tyrosine phosphatase 1B. J Biol Chem 2001;276:47771–47774
16. Salmeen A, Andersen JN, Myers MP, Tonks NK, Barford D. Molecular basis for the dephosphorylation of the activation segment of the insulin receptor by protein tyrosine phosphatase 1B. Mol Cell 2000;6:1401–1412
17. Lee Y, Lee C, Yoon J. Kinetics and mechanisms of DMSO (dimethylsulfoxide) degradation by UV/H(2)O(2) process. Water Res 2004;38:2579–2588
18. Ukkola O, Santaniemi M. Protein tyrosine phosphatase 1B: a new target for the treatment of obesity and associated co-morbidities. J Intern Med 2002;251:467–475
19. Zabolotny JM, Bence-Hanulec KK, Stricker-Krongrad A, et al. PTP1B regulates leptin signal transduction in vivo. Dev Cell 2002;2:489–495
20. Lantz KA, Hart SG, Planey SL, et al. Inhibition of PTP1B by trodusquemine (MSI-1436) causes fat-specific weight loss in diet-induced obese mice. Obesity (Silver Spring) 2009;18:1516–1523
21. Elchebly M, Payette P, Michaliszyn E, et al. Increased insulin sensitivity and obesity resistance in mice lacking the protein tyrosine phosphatase-1B gene. Science 1999;283:1544–1548
22. Brommage R, Desai U, Revelli JP, et al. High-throughput screening of mouse knockout lines identifies true lean and obese phenotypes. Obesity (Silver Spring) 2008;16:2362–2367
23. Ottaway N, Mahbod P, Rivero B, et al. Diet-induced obese mice retain endogenous leptin action. Cell Metab 2015;21:877–882
24. Dodd GT, Decherf S, Loh K, et al. Leptin and insulin act on POMC neurons to promote the browning of white fat. Cell 2015;160:88–104
25. Kusminski CM, Bickel PE, Scherer PE. Targeting adipose tissue in the treatment of obesity-associated diabetes. Nat Rev Drug Discov 2016;15:639–660
26. Kazak L, Chouchani ET, Jedrychowski MP, et al. A creatine-driven substrate cycle enhances energy expenditure and thermogenesis in beige fat. Cell 2015;163:643–655
27. Long JZ, Svensson KJ, Bateman LA, et al. The secreted enzyme PM20D1 regulates lipidated amino acid uncouplers of mitochondria. Cell 2016;166:424–435
28. Keipert S, Kutschke M, Ost M, et al. Long-term cold adaptation does not require FGF21 or UCP1. Cell Metab 2017;26:437–446.e5